Title

Age-Dependent Translocation of Gold Nanoparticles across the Air–Blood Barrier

Journal

ACS Nano, 13(9)

ISSN

1936-0851

Authors

Tsuda, Akira
Donaghey, Thomas C
Konduru, Nagarjun V
et al.

Publication Date

2019-09-24

DOI

10.1021/acsnano.9b03019

Peer reviewed

HHS Public Access

Author manuscript

ACS Nano. Author manuscript; available in PMC 2019 December 24.

Published in final edited form as:

ACS Nano. 2019 September 24; 13(9): 10095–10102. doi:10.1021/acsnano.9b03019.

Age-Dependent Translocation of Gold Nanoparticles across the Air–Blood Barrier

Akira Tsuda[*,†], **Thomas C. Donaghey**[†], **Nagarjun V. Konduru**[†], **Georgios Pyrgiotakis**[†], **Laura S. Van Winkle**[‡], **Zhenyuan Zhang**[†], **Patricia Edwards**[‡], **Jessica-Miranda Bustamante**[‡], **Joseph D. Brain**[†], **Phillip Demokritou**[†]

[†]Department of Environmental Health, Harvard T. H. Chan School of Public Health, Boston, Massachusetts 02115, United States

[‡]Center for Health and the Environment, University of California, Davis, Davis, California 95616, United States

Abstract

Do immature lungs have air–blood barriers that are more permeable to inhaled nanoparticles than those of fully developed mature lungs? Data supporting this notion and explaining the underlying mechanisms do not exist as far as we know. Using a rat model of postnatal lung development, here the data exactly supporting this notion, that is, significantly more gold nanoparticles (NPs) cross from the air space of the lungs to the rest of the body in neonates than in adults, are presented. Moreover, in neonates the translocation of gold NPs is not size dependent, whereas in adult animals smaller NPs cross the air–blood lung barrier much more efficiently than larger NPs. This difference in air–blood permeability in neonate *versus* adult animals suggests that NP translocation in the immature lungs may follow different rules than in mature lungs. Supporting this notion, we propose that the paracellular transport route may play a more significant role in NP translocation in immature animals, as suggested by protein expression studies. Findings from this study are critical to design optimal ways of inhalation drug delivery using NP nanocarriers for this age group, as well as for better understanding of the potential adverse health effects of nanoparticle exposures in infants and young children.

Graphical Abstract

[*]**Corresponding Author** Phone: 617-432-0127. atsuda@hsph.harvard.edu.

Author Contributions

A.T. designed the experiments. T.C.D., N.V.K., G.P., Z.Z., L.S.VW., P.E., J.M.B., and A.T. performed the experiments. T.C.D., N.V.K., G.P., J.D.B., P.D., L.S.VW., P.E., J.M.B., and A.T. reviewed, analyzed, and interpreted the data. A.T. wrote the manuscript. All authors discussed the results and commented on the manuscript.

ASSOCIATED CONTENT

Supporting Information

The Supporting Information is available free of charge on the ACS Publications website at DOI: 10.1021/acsnano.9b03019.

Timeline for lung development in the rodent and human respiratory system; tabulated numerical values plotted in Figure 2 and Figure 3 and 4; nonlinear growths of lung surface area and body weight in infants; extended results of Western blot E-cadherin expression analysis; CytoViva analysis (PDF)

The authors declare no competing financial interest.

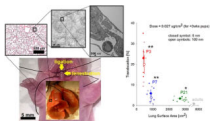

Keywords

nanoparticles; infant; postnatal developing lung; translocation; air–blood lung barrier; paracellular transport route; E-cadherin

Although the human lungs at birth already possess the basic configuration of the fully developed adult lungs (*i.e.,* branched conductive airways followed by the gas exchange portion), structural alveolation occurs mostly postnatally (*i.e.,* in human lungs only 15% of the alveoli are present at birth[1,2]), in addition to a dramatic increase in lung size, which continues until adulthood. Therefore, it is of great interest to identify environmental factors that may influence the morphogenesis[3] and growth of the lungs[4] and also to understand the potential changes in the lung barrier function during lung development,[5] which may underlie potential age-related differences in translocation of nanoparticles and other environmental pollutants.

In previous studies,[6–8] nanoparticle (NP) deposition in the lungs of postnatally developing rats (7, 14, 21, and 35 day old and adults) was determined. It was shown that NP lung deposition *per* body weight was significantly lower in 7-day-old rats but significantly higher for the 21-day-old rat group compared to adult rats. This indicated that NP deposition is strongly age dependent, peaking at the time coinciding with the end of bulk alveolation (21 days).

The present study was designed to systematically assess NP translocation *via* the lungs' air–blood tissue barrier in infant animals at various ages by employing intratracheal instillation in order to avoid GI tract ingestion of nanoparticles *via* particle deposition in the nasopharynx. We also avoided nanoparticle transport from the large airways by mucociliary escalator to the GI tract (see detailed explanation below). We selected three time points in postnatal development (three age groups) that represent important stages of the development of alveolar structures[9] (see Figure S1 in the Supporting Information, where we made lung developmental time comparison between humans and rodents): the beginning of alveolation (3-day-old rats; equivalent to human preterm babies), the bulk of alveolation (7-day-old rats; human newborns), and the end of the bulk alveolation (21-day-old rats; human toddlers). We used polyvinylpyrrolidone (PVP)[10]-coated spherical gold nanoparticles (AuNPs) of two sizes (5 and 100 nm) as a nanoparticle model (see Figure 1a–d). A cut-down tracheotomy was performed, and immediately before tracheal instillation, the trachea above fenestration was ligated to avoid mucociliary clearance (Figure 1e). AuNPs were intratracheally instilled *via* a polyethylene tubing since precise dosing by inhalation in the small infant animals is practically impossible (see the detailed discussion in Semmler-Behnke *et al.,* 2012) Although the local distribution of NPs in the lungs is likely to be different after instillation and inhalation,[11] these two modes of NP administration yield comparable measurements in terms of overall NP translocation (data not shown). The NPs were instilled during

inspiration, instead of expiration, to ensure that all the NPs were indeed delivered into the lungs (Figure 2, CytoViva images). It is also worth noting that the administered dose of NPs was determined based on lung surface area, which is more appropriate if considering the total burden to the body, instead of body weight (which is usually employed in toxicological studies), because the lung surface area is dramatically changing during lung development and the ratio of the lung surface area to body weight in developing rats is very different from that in the adults (see Figure S2 in the Supporting Information, where we demonstrated a nonlinear relationship between body weight and lung surface area during the lung development). A dose of 0.027 μg per unit lung surface area (cm^2) was employed, as this dose was found not to cause lung injury and inflammation (see below). The animals were kept in a box placed on a heated pad to maintain optimal body temperature and breathed anesthetic gas (1.5–3% isoflourane) for 3 h (Figure 1g). After 3 h in the box, the animals were sacrificed by exsanguination, and the lungs were excised. The amounts of gold in the lungs and in extrapulmonary tissues were measured by inductively coupled plasma mass spectrometry (ICP-MS) in order to determine the NP translocation. It is important to note that all the gold found in the tissues outside the lungs must have translocated solely *via* the pulmonary air–blood tissue barrier because the pulmonary system and the GI system had been separated by tracheal ligation before the administration of NPs into the lungs.

RESULTS AND DISCUSSION

The findings showed that the systemic translocation of NPs in infants was age dependent and significantly different from that of adult animals. More specifically, it was demonstrated that the translocation of NPs in infant animals was significantly higher than that of mature ones (Figure 3, Table S1 in the Supporting Information. Table S1 provides the numerical values of data plotted in Figure 3). The translocation in the 3-day-old (P3), 7-day-old (P7), and the 21-day-old (P21) rats reached more than 23%, 6%, and 3%, respectively. It is also worth noting that the miniscule 3% of translocated NPs found for the P21 rat group is still statistically significantly higher than the ≤1% for adults[8,12,13] (>90 days). It was also demonstrated that there was no size dependency in the translocation on NPs in infant animals. This important finding is in contrast to what has been previously reported in adults, [8,12,13] where the translocation of NPs was consistently size-dependent (*i.e.,* smaller NPs translocated more efficiently than larger ones). (The focus of this study was AuNP translocation in neonatal and developing animals; we did not aim to repeat previously conducted studies on NP translocation in adult animals,[8,12,13] which reported size dependency. In other words, in this study, adults were only used to illustrate the point that the fraction of NPs translocating in adult animals is very small compared to that in neonates or developing animals.)

It is worth noting that in order to exclude the possibility that the high translocation across the air–blood tissue barrier observed in immature animals was due to extensive lung injuries that compromise the air–blood barrier as a consequence of NP exposure, the epithelial tissue injury was assessed for the P3 rat group using both histopathology and biochemical analysis of bronchoalveolar lavage fluids (BALF) of both NP exposed and unexposed (control) animals (Figure 4). Figure 4a shows no gross morphological indicators of lung damage or obvious histopathological differences. Similarly, lactate dehydrogenase (LDH) levels in the

BAL, which indicate lung injury, were measured in samples of the three groups (P3, P7, P21, $n = 5$ each group), and the results show no significant differences for NP-exposed and control animals (Figure 4b; Table S2 in the Supporting Information provides the numerical values of data plotted in Figure 4b). [We note that lung overload is a complicated phenomenon[16–18] and is currently understudied. Based on the publication by Morrow et al.,[19,20] for rats and insoluble particles such as the AuNPs used in this study, the impairment/overload starts when the average phagocytized volume of alveolar macrophages (AM) exceeds 6% of the normal AM load and that complete cessation of clearance occurs when the phagocytized volume reaches 60% of the normal AM volume. Unfortunately, these parameters have not been studied in neonatal rats, and thus application of these Morrow parameters is not possible. Nevertheless, the dose of particles we selected was very small (0.027 $\mu g/cm^2$) and did not cause any lung injury and inflammation, as demonstrated by histopathology and BAL enzyme values (see in Figure 4). At the same time, the dose was high enough that gold concentrations could be measured in our samples. Thus, we concluded that the dose used most likely did not reach lung overload levels in the neonatal rats.]

In our previous study,[21] we found that the numbers of alveolar macrophages in neonatal animals did not reach the fully developed adult values, and their functions [two main functions of AMs are phagocytic ability and generation of reactive oxygen species (ROS)] are still immature, especially in the early developmental stage. Although the production of reactive oxidants by AMs is beneficial in killing invading microorganisms, it is potentially detrimental to nearby tissue.[22,23] It has been suggested that there is a coupling between functional maturity of the cellular defense system and morphological maturity of the lung parenchyma. For instance, in rats, AMs attained full oxidant-releasing capacity only once the major period of postnatal alveolar morphogenesis had been completed.[24]

Due to the lower number of AMs and their immature function, it is possible that inhaled NPs go across the air–blood barrier into the bloodstream without significantly activating AMs in the developing lungs.

The high NP translocation in 3-day-old rats (~23%) progressively decreased with age and reached the low levels typically characteristic for adults[8,12,13] (≤1%). These findings and the observation that 5 and 100 nm NPs translocated with equal efficiency in infants are consistent with the hypothesis that potential paracellular transport[5] of NPs may also be significantly involved in the NP translocation process in immature animals. Epithelial cells are connected with each other by complex structures forming cell–cell junctions that include tight junctions, adherent junctions, gap junctions, and desmosomes. Among many adhesion molecules, E-cadherin is a key component of cell–cell junctions and plays a crucial role in the formation of tight junction.[25–27] E-cadherin is expressed as an inactive pro-peptide precursor, which undergoes proteolytic cleavage to become a functionally active protein. In order to test whether the E-cadherin expression and maturation differ in infant lungs *versus* adult ones, the E-cadherin levels were compared in the lung tissues of 7-day-old ($n = 5$) and adult rats ($n = 4$) (Figure 5). It is worth noting that the pro-E-cadherin precursor protein is 94 kDa in size, and it is cleaved by furin-like and other proteases[28,29] to result in the formation of the functionally active mature polypeptide of 80 kDa. Western blot analysis showed the presence of the 94 kDa pro-E-cadherin precursor, but no cleavage product in the samples of

7-day-old rat lungs, whereas in all the samples prepared from adult lungs a band representing the 80 kDa mature cadherin cleavage product was seen (see Figure S3 in the Supporting Information, where all data from $n = 5$ of 7-day-old rats and $n = 4$ adults rats are shown), in addition to various amounts of the 94 kDa pro-E-cadherin, suggesting the absence of E-cadherin processing in infant lungs. Differences in the activities of proteases, which play critical roles in shaping the lung architecture during development, in immature *versus* adult lungs may underlie the findings of the present study. We also compared the expression of an important component of the tight junctions, zonula occludens-1 protein (ZO-1), between 7-day-old rat lungs *versus* adult lungs (5 and 4 samples, respectively). Although the difference in the ZO-1 expression between infant and adult rats was not statistically significant, the ZO-1 expression in infant lungs on average was lower than that of adult lungs. Taken together, these results are consistent with our hypothesis that the epithelial barrier and its components including the tight junctions are functionally different in developing *versus* adult lungs and suggest the involvement of paracellular transport of NPs in infant animals.

CONCLUSION

In summary, the key findings of this study are (i) NP translocation from lungs to the rest of the body is significantly higher in infant animals than that in adults; (ii) the NP translocation decreases with age; thus infancy can be considered as a critically vulnerable window in terms of NP translocation *via* lungs, as shown in epidemiological studies related to ambient ultrafine particles:[4,30–32] (iii) the lack of difference in the translocation between 5 nm *versus* 100 nm AuNPs in infants, in contrast to what is observed for adults that experience size-dependent translocation,[8,12,13] suggests that there may be a significant involvement of paracellular transport in the structurally immature lungs compared to the adults. This hypothesis is supported by our findings of age-dependent differences in the expression of some key proteins that contribute to the formation of epithelial cell junctions.

Finally, these findings have important implications for the assessment of the potential toxicity of inhaled nanosize particles of both environmental and engineered origins. With the increased use of engineered nanoparticles in many products, inhalation exposures are inevitable.[33–40] In particular, for infants, the physical and chemical contacts of NPs with the developing lungs represent insults that may damage lung development and long-term lung function[4,41] and may lead to increased infant mortality.[31,32] Indeed, infancy has been recognized as one of the most vulnerable ages for adverse health effects caused by inhaled particles.[41,42] Our study shows that a considerable amount of inhaled nanoparticles can cross the tissue barrier of the infant lungs; thus in addition to damaging the lungs locally, these particles will become systemic and reach organs beyond the lungs. As the translocation is dramatically higher in infants, the risk of nanosize-particle-mediated damage throughout the body is potentially higher in this age group than in others.

On the other hand, the large surface area of the lungs is an attractive site for delivery of pulmonary and systemic inhalation therapies.[43,44] In this sense, the enhanced capacity of infant lungs to allow NPs to translocate and become systemic provides an opportunity for

the judicious design of optimal inhalation drug delivery using nanocarrier systems for this age group.

Further understanding of both NP lung deposition[6–8] and fate (translocation) at various stages of the postnatal lung development is crucial for both advancing our understanding of potential adverse health effects of inhaled nanoparticles and developing nanotechnology-based drug delivery strategies for infants.

MATERIALS AND METHODS

Animals.

Lactating Wistar rats with 1-day-old pups delivered normally were purchased from Charles River Laboratories (Wilmington, MA, USA). The animals were maintained on a 12 h light/dark cycle in microisolator cages within the animal care facility of the Harvard T. H. Chan School of Public Health. The mother rats were fed commercial rodent food pellets and water *ad libitum*. The animals were treated in accordance with all local, state, federal, and institutional guidelines consistent with animal protocols approved by the Animal Care and Use Committee overseeing the animal facility.

At the chosen experimental ages (3 days, 7 days, and 21 days after birth), the pups were removed from their mothers and used for the experiments. The litter size was approximately 10 pups. No distinction was made regarding the sex of the pups used. Growth rate and lung development are not thought to differ significantly between males and females up to the time of weaning (21 days).[45]

A minimum of five animals per the two particle sizes and three time points was used for each group and subsequent analyses. Gold concentration was measured by ICP-MS (see below). Similarly, a minimum of five animals per particle size and time point were used for the LDH analyses (see below). Five animals per particle size and designated animal age were used for histopathology (Figure 4) and Western blot (Figure 5) analyses.

Nanoparticles and Characterization of NP Suspensions for Animal Studies.

Spherical gold nanoparticles of ~5 nm (*i.e.,* 5.7 ± 1.247 nm) and ~100 nm (*i.e.,* 128.3 ± 0.4 nm) in size in solution (water) were purchased from nanoComposix (San Diego, CA, USA). The AuNPs of both sizes were coated with PVP to prevent aggregation.[10] In previous studies performed on adult animals, NP size was identified as one of the most important parameters affecting translocation across the air–blood barrier.[8,12,13] NP size was characterized in suspension using various techniques (*e.g.,* DC, DLS, TEM) as outlined previously.[38] The morphology of AuNPs was examined by transmission electron microscopy (TEM) (Figure 1a,b). The size distribution of AuNPs in water solution was measured by dynamic light scattering (DLS, Zetasizer Nano ZS, Malvern, UK), and the hydrodynamic diameter (d_H) distribution was calculated (Figure 1c,d). Zeta potential and ionic strength of AuNPs were also measured by DLS before the administration of AuNPs to the animals. As DLS is not suitable for nanoparticles less than 10 nm, a disc centrifuge (CPS Instruments, Prairieville, LA, USA) was used to confirm the size of 5 nm particles (see Figure 1 legend for additional details[46]).[46]

Dose.

The dose to be administered by intratracheal instillation was determined as follows. When the AuNPs were purchased as an aqueous suspension, the concentration selected was 1 μg/μL. We reasoned that the volume of the instilled suspension should be large enough to allow a wide distribution when delivered to the lungs,[11] but small enough not to disturb breathing. The instillation volume was set at 1 μL per g body weight. The total dose delivered was calculated based on the lung surface area, which is strongly age-dependent (see Figure S2 in the Supporting Information, where we demonstrated a nonlinear relationship between body weight and lung surface area during lung development). The dose of AuNPs administered (0.027 μg/cm^2) was selected to be low enough not to cause lung injury and inflammation[16] but high enough for accurate ICP-MS detection.

NP Exposure.

The rat pups were anesthetized with 4% isoflurane, and a cutdown tracheotomy was performed. Two suture threads were placed just above and below fenestration (Figure 1e), and the trachea was ligated above the fenestration, immediately before the tracheal instillation (a suture thread below fenestration was used later). The animals breathed anesthetic gas through the trachea fenestration; PVP-coated AuNPs of 5 or 100 nm were intratracheally instilled *via* PolyE 140 polyethylene tubing (Harvard Apparatus, Smith Medical International, Kent, UK) during the inspiration phase. The animals were kept at a body temperature of 36 °C and breathed anesthetic gas (1.5–3% isoflurane) for 3 h (Figure 1g) before being sacrificed by exsanguination. Then the trachea was tied by the second suture thread, and the lungs were excised. The lungs and the extrapulmonary tissues were separated and stored at 4 °C for subsequent ICP-MS analyses.

NP Measurements.

The amount of gold in the lungs and extrapulmonary tissues was measured by ICP-MS (at the UW-Madison and Wisconsin State Laboratory of Hygiene Trace Element Research Group, Madison, WI, USA), and the translocation efficiency across the air–blood barrier was calculated from these two values.

Measurement of Lung Injury.

Rats were exposed to NPs as described above. After the animals were sacrificed, bronchoalveolar lavage (BAL) from the samples of the three groups (P3, P7, P21, $n = 5$ each group) was performed with phosphate-buffered saline (PBS) using a volume of 80% total lung capacity (TLC) twice. The supernatant of the BAL fluid was analyzed for LDH as an indicator of tissue injury (see Table S2 in the Supporting Information, where the numerical values of data plotted in Figure 4b are given).

Protein Samples.

The expression of E-cadherin and zonula occludens-1 (tight junction protein-1) in the lungs of 7-day-old and adult rats ($n = 5$ and $n = 4$, respectively) was studied. The lungs of the animals were excised and homogenized with glass/Teflon dounces in 10 mL (adult lungs) or 4 mL (“pup” lungs) of SDS boiling buffer without reducing agents. The samples were then

heated in a boiling water bath for 7 min. The samples were centrifuged to remove insoluble material, and the protein concentrations of the supernatants were determined using the BCA assay.[47] The samples were then diluted to 4 mg/mL in buffer "O" (10% glycerol (w/v), 50 mM dithiothreitol, 2.3% SDS (w/v), and 62.5 mM tris, pH 6.8 at 23 °C) and heated in a dry bath at 95 °C for 10 min before loading.

Western Blot Procedure.

Acrylamide gels were run according to the method of Laemmli as reported by O'Farrell.[48,49] Samples were loaded in lanes in a stacking gel made of polyacrylamide on top of a 10% acrylamide slab gel (0.75 mm thick). SDS gel electrophoresis was carried out for about 3.5 h at 15 mA/gel. The gel was then placed in transfer buffer (10 mM CAPS, pH 11.0, 10% MeOH) and blotted onto PVDF membrane (Thermo Fisher Scientific, Waltham, MA, USA) overnight at 225 mA and approximately 100 V/two gels. The following proteins (MilliporeSigma, Burlington, MA, USA) were used as molecular weight standards: myosin (220 000 Da), phosphorylase A (94 000), catalase (60 000), actin (43 000), carbonic anhydrase (29 000), and lysozyme (14 000). The PVDF membrane was destained in 100% methanol and rinsed briefly in tris-tween-buffer-saline (TTBS). The blot was blocked for 2 h in 5% nonfat-dried milk (NFDM) diluted in TTBS. The blot was then incubated in primary antibody (anti-E-Cadherin [Novus, cat no. NBP2–16258, lot no. 42564] diluted 1:20 000 in 2% NFDM TTBS or anti-Tight Junction Protein [Novus, cat no. NBP1–91621, lot no. QC5556–41620] diluted 1:500 in 2% NFDM TTBS) overnight and rinsed 3 × 10 min in TTBS. The blot was then placed in secondary antibody (anti-rabbit IgG-HRP [SeraCare, cat no. 5220–0337, lot no. 10245261] diluted 1:20 000 in 2% NFDM TTBS) for 2 h, rinsed as above, treated with ECL (Thermo, cat no. 32106), and exposed to X-ray film (GE Amersham Hyperfilm ECL, cat no. 28906839). Subsequently, the blots were blocked again for 2 h in 5% NFDM TTBS and probed for β actin by incubating them in anti-β actin antibodies [Abcam, cat no. ab8227, lot no. GR3188015–2] diluted to 0.01 μg/mL in 2% NFDM TTBS) overnight, and they were rinsed 3 × 10 min in TTBS. The blots were then placed in secondary antibody (anti-rabbit IgG-HRP [SeraCare, cat no. 5220–0337, lot no. 10245261] diluted 1:20 000 in 2% NFDM TTBS) for 2 h, rinsed as above, treated with ECL (Thermo, cat no. 32106), and exposed to X-ray film (GE Amersham Hyperfilm ECL, cat no. 28906839).

CytoViva.

Gold nanoparticles in lung tissue were imaged using a CytoViva enhanced dark-field microscope (CytoViva, Auburn, AL, USA). Gold particles where evaluated in unstained paraffin-embedded lung sections at 60× magnification. Spectral analysis of AuNP was performed utilizing hyperspectral dark-field microscopy (CytoViva). To generate a mean spectral profile of AuNP, particles were diluted to 250 μg/mL in water, loaded onto clean glass microscope slides, and cover slipped in an aqueous mounting medium (Vector, Vectamount AQ H-5501). Mean spectra were created using pixels with an intensity greater than 2000. To determine a mean spectrum from gold nanoparticles in lung tissue, a minimum of 1000 pixels of AuNP in the tissue were collected to form a region of interest. This spectrum was then compared with the suspended gold particle control and the lung

tissue without localized AuNPs (for additional information about CytoViva see the Supporting Information).

Histopathology.

To examine the gross morphology of lung tissue, the lungs of the 3-day-old, 7-day-old, and 21-day-old rats exposed to 5 and 100 nm AuNPs were fixed at 80% TLC with glutaraldehyde and stained with hematoxylin and eosin.

Transmission Electron Microscopy.

TEM was used for two purposes: to examine the morphology of nanoparticles used (Figure 1a,b) and the ultrastructure of the lungs. To examine the ultrastructure of the lungs of the 3-day-old, 7-day-old, and 21-day-old rats exposed to 5 and 100 nm AuNPs the lungs were fixed at 80% TLC with 2.5% glutaraldehyde. Small pieces (1–2 mm cubes) of tissue from a perfusion fixed animal were postfixed for at least 2 h at room temperature in 2.5% glutaraldehyde, 1.25% paraformaldehyde, and 0.03% picric acid in 0.1 M sodium cacodylate buffer (pH 7.4), washed in 0.1 M cacodylate buffer, treated with 1% osmium tetroxide (OsO_4)/1.5% potassium ferrocyanide ($KFeCN_6$) for 1 h, washed in water twice, then in 50 mM maleate buffer pH 5.15 (MB), and incubated in 1% uranyl acetate in MB for 1 h followed by one wash in MB, two washes in water, and subsequent dehydration in graded alcohol dilutions (10 min each; 50%, 70%, 90%, 2 × 10 min 100%). The samples were then put in propylene oxide for 1 h and infiltrated overnight in a 1:1 mixture of propylene oxide and TAAB Epon (TAAB Laboratories Equipment Ltd., https://taab.co.uk). The following day the samples were embedded in TAAB Epon and polymerized at 60 °C for 48 h. Ultrathin sections (about 80 nm) were cut on a Reichert Ultracut-S microtome, picked up onto copper grids stained with lead citrate, and examined in a JEOL 1200EX transmission electron microscope or a TecnaiG^2 Spirit BioTWIN. Images were recorded with an AMT 2k CCD camera.

Statistical Analyses.

The small symbols in Figure 2 represent individual data; the large symbols represent the average ± one standard deviation of translocation measurement (vertical variation) and lung surface area calculations (horizontal variation) for each age group. Statistical significance was determined by ANOVA, and *P* values of 0.01 or 0.05 are indicated. Segmented regression[14,15] shows the lack of difference in translocation of 5 nm *vs* 100 nm AuNPs in the developing lungs.

Supplementary Material

Refer to Web version on PubMed Central for supplementary material.

ACKNOWLEDGMENTS

This study was supported, in part, by NIH Grants HL094567, ES000002, S10OD021780, P30ES023513, K99ES025813, and NSF15–022. We thank R. Molina for his discussions and help. We also would like to acknowledge R. Anderson for her technical assistance.

REFERENCES

(1). Hislop AA; Wigglesworth JS; Desai R. Alveolar Development in the Human Fetus and Infant. Early Hum. Dev 1986, 13, 1–11. [PubMed: 3956418]

(2). Herring MJ; Putney LF; Wyatt G; Finkbeiner WE; Hyde DM Growth of Alveoli during Postnatal Development in Humans Based on Stereological Estimation. Am. J. Physiol. Lung Cell Mol. Physiol 2014, 307, L338–L344. [PubMed: 24907055]

(3). Rawlins EL; Okubo T; Que J; Xue Y; Clark C; Luo X; Hogan BL Epithelial Stem/Progenitor Cells in Lung Postnatal Growth, Maintenance, and Repair. Cold Spring Harbor Symp. Quant. Biol 2008, 73, 291–295.

(4). Gauderman WJ; Urman R; Avol E; Berhane K; McConnell R; Rappaport E; Chang R; Lurmann F; Gilliland F. Association of Improved Air Quality with Lung Development in Children. N. Engl. J. Med 2015, 372, 905–913. [PubMed: 25738666]

(5). Vyas-Read S; Vance RJ; Wang W; Colvocoresses-Dodds J; Brown LA; Koval M. Hyperoxia Induces Paracellular Leak and Alters Claudin Expression by Neonatal Alveolar Epithelial Cells. Pediatr. Pulmonol. 2018, 53, 17–27.

(6). Semmler-Behnke M; Kreyling WG; Schulz H; Takenaka S; Butler JP; Henry FS; Tsuda A. Nanoparticle Delivery in Infant Lungs. Proc. Natl. Acad. Sci. U. S. A 2012, 109, 5092–5097. [PubMed: 22411799]

(7). Das GK; Anderson DS; Wallis CD; Carratt SA; Kennedy IM; Van Winkle LS Novel Multi-Functional Europium-Doped Gadolinium Oxide Nanoparticle Aerosols Facilitate the Study of Deposition in the Developing Rat Lung. Nanoscale 2016, 8, 11518–11530.

(8). Kreyling WG; Möller W; Holzwarth U; Hirn S; Wenk A; Schleh C; Schäffler M; Haberl N; Gibson N; Schittny JC Age-Dependent Rat Lung Deposition Patterns of Inhaled 20 Nanometer Gold Nanoparticles and their Quantitative Biokinetics in Adult Rats. ACS Nano 2018, 12, 7771–7790. [PubMed: 30085651]

(9). Burri PH Development and Growth of the Human Lung. In Handbook of Physiology Section 3: The Respiratory System; Fishman AP, Fisher AB, Eds.; William & Wilkins: Baltimore, 1985; pp 1–46.

(10). Dreaden EC; Alkilany AM; Huang X; Murphy CJ; El-Sayed MA The Golden Age: Gold Nanoparticles for Biomedicine. Chem. Soc. Rev 2012, 41, 2740–2779. [PubMed: 22109657]

(11). Osier M; Oberdörster G. Intratracheal Inhalation vs Intratracheal Instillation: Differences in Particle Effects. Fundam. Appl. Toxicol 1997, 40, 220–227. [PubMed: 9441718]

(12). Choi HS; Ashitate Y; Lee JH; Kim SH; Matsui A; Insin N; Bawendi MG; Semmler-Behnke M; Frangioni JV; Tsuda A. Rapid Translocation of Nanoparticles from the Lung Airspaces to the Body. Nat. Biotechnol 2010, 28, 1300–1303. [PubMed: 21057497]

(13). Kreyling WG; Hirn S; Möller W; Schleh C; Wenk A; Celik G; Lipka J; Schäffler M; Haberl N; Johnston BD; Sperling R; Schmid G; Simon U; Parak WJ; Semmler-Behnke M. Air-Blood Barrier Translocation of Tracheally Instilled Gold Nanoparticles Inversely Depends on Particle Size. ACS Nano 2014, 8, 222–223. [PubMed: 24364563]

(14). Das R; Banerjee M; Nan B; Zheng H. Fast Estimation of Regression Parameters in a Broken-Stick Model for Longitudinal Data. J. Am. Stat. Assoc 2016, 111, 1132–1143. [PubMed: 28316356]

(15). Nummi T; Virtanen P; Leino-Arjas P; Hammarström A. Trajectories of a Set of Ten Functional Somatic Symptoms from Adolescence to Middle Age. Arch. Public Health 2017, 75, 11. [PubMed: 28286651]

(16). Borm P; Flemming CR; Oberdörster G. Lung Particle Overload: Old School – New Insights? Part. Fibre Toxicol 2015, 12, 10. [PubMed: 25927223]

(17). Pauluhn J. Derivation of Occupational Exposure Levels (OELs) of Low-Toxicity Isometric Biopersistent Particles: How Can the Kinetic Lung Overload Paradigm be Used for Improved Inhalation Toxicity Study Design and OEL-Derivation? Part. Part. Fibre Toxicol 2014, 11, 72. [PubMed: 25526747]

(18). Morfeld P; Bruch J; Levy L; Ngiewich Y; Chaudhuri I; Muranko H; Myerson R; McCunney RJ Translation Toxicology in Setting Occupational Exposure Limits for Dusts and Hazard

Classification- a Critical Evaluation of a Recent Approach to Translate Dust Overload Findings from Rats to Humans. Part. Fibre Toxicol 2015, 12, 3. [PubMed: 25925672]

(19). Morrow PE Possible Mechanisms to Explain Dust Overloading of the Lungs. Fundam. Appl. Toxicol 1988, 10, 369–384. [PubMed: 3286345]

(20). Oberdörster G; Ferin J; Morrow PE Volumetric Loading of Alveolar Macrophages (AM): A Possible Basis for Diminished AM-Mediated Particle Clearance. Exp. Lung Res 1992, 18, 87–104. [PubMed: 1572327]

(21). Dickie R; Tasat DR; Fernandez Alanis E; Delfosse V; Tsuda A. Age-Dependent Changes in Porcine Alveolar Macrophage Function during the Postnatal Period of Alveolarization. Dev. Comp. Immunol 2009, 33, 145–151. [PubMed: 18775449]

(22). Babior BM Phagocytes and Oxidative Stress. Am. J. Med 2000, 109, 33–44. [PubMed: 10936476]

(23). Fernandez ML; Duran HA; O'Connor SE; Cabrini RL; Molinari BL Role of Distinct Subpopulations of Peritoneal Macrophages in the Regulation of Reactive Oxygen Species Release. Free Radical Biol. Med 1999, 27, 797–809. [PubMed: 10515584]

(24). Delacourt C; d'Ortho MP; Macquin-Mavier I; Pezet S; Housset B; Lafuma C; Harf A. Oxidant-Antioxidant Balance in Alveolar Macrophages from Newborn Rats. Eur. Respir. J 1996, 9, 2517–2524. [PubMed: 8980963]

(25). Gumbiner B; Stevenson B; Grimaldi A. The Role of the Cell Adhesion Molecule Uvomorulin in the Formation and Maintenance of the Epithelial Junctional Complex. J. Cell Biol. 1988, 107, 1575–1587. [PubMed: 3049625]

(26). Watabe M; Nagafuchi A; Tsukita S; Takeichi M. Induction of Polarized Cell-Cell Association and Retardation of Growth by Activation of the E-Cadherin-Catenin Adhesion System in a Dispersed Carcinoma Line. J. Cell Biol. 1994, 127, 247–256. [PubMed: 7929567]

(27). Nawijn MC; Hackett TL; Dirkje S; Postma DS; van Oosterhout AJM; Heijink IH E-cadherin: Gatekeeper of Airway Mucosa and Allergic Sensitization. Trends Immunol. 2011, 32, 248–255. [PubMed: 21493142]

(28). Posthaus H; Dubois CM; Laprise MH; Grondin F; Suter MM; Muëller E. Proprotein Cleavage of E-Cadherin by Furin in Baculovirus Over-Expression System: Potential Role of Other Convertases in Mammalian Cells. FEBS Lett. 1998, 438, 306–310. [PubMed: 9827567]

(29). van Roy F; Berx G. The Cell-Cell Adhesion Molecule E-Cadherin. Cell. Mol. Life Sci 2008, 65, 3756–3788. [PubMed: 18726070]

(30). Lelieveld J; Pöschl U. Chemists can Help to Solve the Air-Pollution Health Crisis. Nature 2017, 551, 291–293. [PubMed: 29144470]

(31). Glinianaia SV; Rankin J; Bell R; Pless-Mulloli T; Howel D. Does Particulate Air Pollution Contribute to Infant Death? A Systematic Review. Environ. Health Perspect 2004, 112, 1365–1370. [PubMed: 15471726]

(32). Heft-Neal S; Burney J; Bendavid E; Burke M. Robust Relationship between Air Quality and Infant Mortality in Africa. Nature 2018, 559, 254–258. [PubMed: 29950722]

(33). Kessler R. Engineered Nanoparticles in Consumer Products: Understanding a New Ingredient. Environ. Health Perspect 2011, 119, a120–a125. [PubMed: 21356630]

(34). Som C; Nowack B; Krug HF; Wick P. Toward the Development of Decision Supporting Tools that can be Used for Safe Production and Use of Nanomaterials. Acc. Chem. Res 2013, 46, 863–872. [PubMed: 23110540]

(35). Pirela SV; Miousse IR; Lu X; Castranova V; Thomas T; Qian Y; Bello D; Kobzik L; Koturbash I; Demokritou P. Effects of Laser Printer-Emitted Engineered Nanoparticles on Cytotoxicity, Chemokine Expression, Reactive Oxygen Species, DNA Methylation, and DNA Damage: a Comprehensive In Vitro Analysis in Human Small Airway Epithelial Cells, Macrophages, and Lymphoblasts. Environ. Health Perspect 2016, 124, 210–219. [PubMed: 26080392]

(36). Pyrgiotakis G; Vedantam P; Cirenza C; McDevitt J; Eleftheriadou M; Leonard S; Demokritou P. Optimization of a Nanotechnology based Antimicrobial Platform for Food Safety Applications using Engineered Water Nanostructures (EWNS). Sci. Rep 2016, 6, 1–12. [PubMed: 28442746]

(37). Tsuda A; Konduru NV Engineered Nanoparticles in the Lungs: from Interaction with Bio-Molecules to Protein Corona. NanoImpact 2016, 2, 38–44. [PubMed: 29202111]

(38). Watson CY; DeLoid GM; Pal A; Demokritou P. Buoyant Nanoparticles: Implications for Nano-Biointeractions in Cellular Studies. Small 2016, 12, 3172–3180. [PubMed: 27135209]

(39). Eleftheriadou M; Pyrgiotakis G; Demokritou P. Nanotechnology to the Rescue: Using Nano-Enabled Approaches in Microbiological Food Safety and Quality. Curr. Opin. Biotechnol 2017, 44, 87–93. [PubMed: 27992831]

(40). Konduru NV; Molina RM; Swami A; Damiani F; Pyrgiotakis G; Lin P; Andreozzi P; Donaghey TC; Demokritou P; Krol S; Kreyling WG; Brain JD Protein Corona: Implications for Nanoparticle Interactions with Pulmonary Cells. Part. Fibre Toxicol 2017, 14, 42. [PubMed: 29084556]

(41). WHO 2017, http://www.who.int/ceh/publications/ceh-Infographics-2017-english.pdf?ua=1, accessed on 10/23/2018.

(42). Waller LA Infant Deaths from Air Pollution Estimated. Nature 2018, 559, 188–189. [PubMed: 29988051]

(43). Everard ML Inhalation Therapy for Infants. Adv. Drug Delivery Rev. 2003, 55, 869–878.

(44). DiBlasi RM Clinical Controversies in Aerosol Therapy for Infants and Children. Respir. Care 2015, 60, 894–916.

(45). Kohn DF; Clifford CB Biology and Diseases of Rats. In Laboratory Animal Medicine; Fox JG, Anderson LC, Loew FM, Quimby FW, Eds.; Academic: New York, 2002; pp 121–165.

(46). DeLoid GM; Cohen JM; Pyrgiotakis G; Demokritou P. Preparation, Characterization, and In Vitro Dosimetry of Dispersed, Engineered Nanomaterials. Nat. Protoc 2017, 12, 355–371. [PubMed: 28102836]

(47). Smith PK; Krohn RI; Hermanson GT; Mallia AK; Gartner FH; Provenzano MD; Fujimoto EK; Goeke NM; Olson BJ; Klenk DC Measurement of Protein Using Bicinchoninic Acid. Anal. Biochem 1985, 150, 76–85. [PubMed: 3843705]

(48). Laemmli UK Cleavage of Structural Proteins during the Assembly of the Head of Bacteriophage T4. Nature 1970, 227, 680–685. [PubMed: 5432063]

(49). O'Farrell PH High Resolution Two-Dimensional Electrophoresis of Proteins. J. Biol. Chem 1975, 250, 4007–4021. [PubMed: 236308]

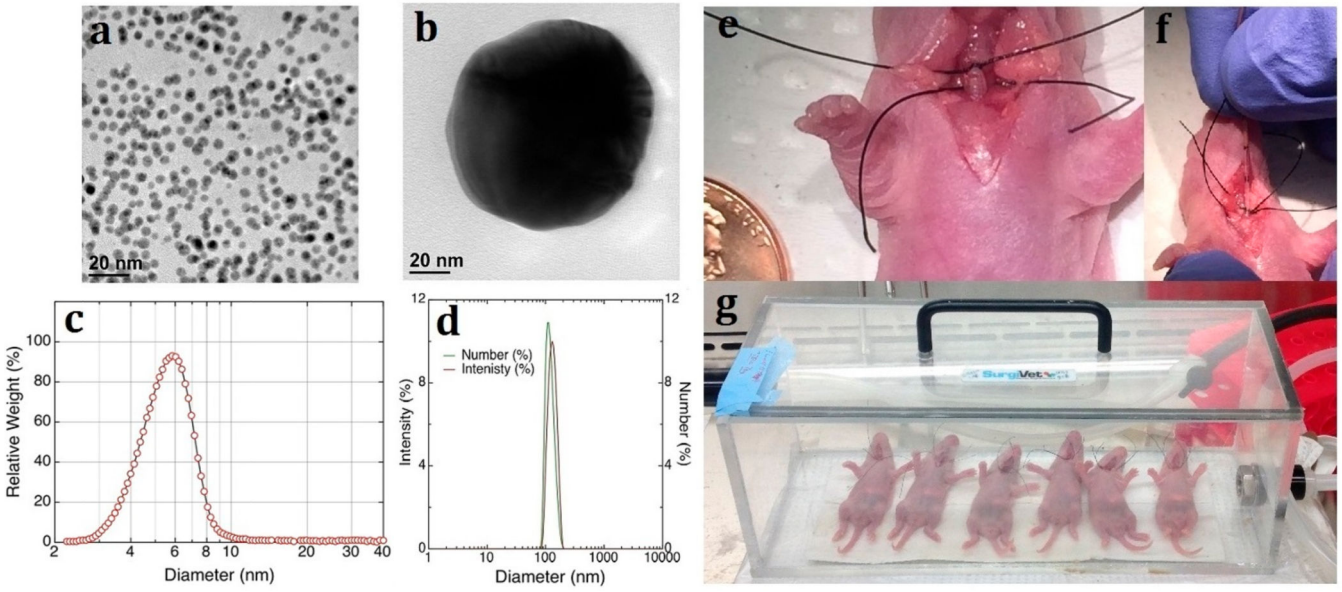

Figure 1.

Experimental setup. Gold nanoparticles (AuNPs) of 5 and 100 nm in size in suspension (water) were purchased from nanoComposix (San Diego, CA, USA). (a, b) Morphology of 5 and 100 nm polyvinylpyrrolidone (PVP)-coated BioPure AuNPs by TEM. PVP is a water-soluble polymer, and coating AuNPs with PVP prevents aggregation.[10] (c) Size distribution of 5 nm AuNPs measured by disc centrifuge (CPS Instruments, Prairieville, LA, USA). The hydrodynamic diameter (d_H) was 5.7 ± 1.247 nm. (d) Intensity (crimson line) and size distribution (green line) of 100 nm AuNPs in water solution measured by dynamic light scattering (Zetasizer Nano ZS, Malvern, UK.). The d_H was 128.3 ± 0.4 nm (PDI = 0.031 ± 0.004). Zeta-potentials of PVP-coated AuNPs were also measured as −15.1 ± 5.81 mV (for 5 nm AuNPs) and −26.1 ± 3.0 mV (for 100 nm AuNPs). (e) Trachea of rats above fenestration was ligated before exposure to NPs to avoid mucociliary clearance. (f) AuNPs were instilled during inspiration. (g) Translocation was allowed to occur for 3 h.

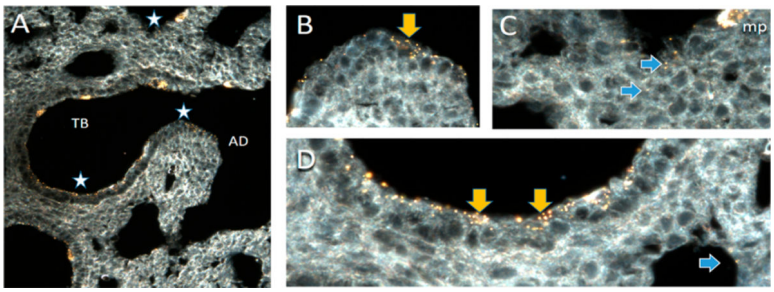

Figure 2.

CytoViva dark-field microscopy of AuNPs (100 nm) in the lung of a 3-day-old rat following instillation exposure. NPs localize throughout the terminal bronchiole (TB) and alveolar duct (AD). (A) Overview of region of terminal bronchiole alveolar duct junction. Regions with stars are presented at 60× magnification in B–D. (B) Epithelium lining the transitional region between the end of a terminal bronchiole and the beginning of the alveolar duct contains abundant NPs visible as yellow dots and agglomerates both on the cell surface and within the epithelium (yellow arrow). (C) NPs in the alveoli (blue arrows). An alveolar macrophage (mp) in the upper right corner of the image contains abundant NPs. (D) NPs on the surface and penetrating into the epithelium of the terminal bronchiole (yellow arrows) and the alveolus (blue arrow). Control tissues did not have particles. Particles were confirmed to be AuNPs using hyperspectral imaging (data not shown) of AuNPs to provide reference spectra, which were then mapped onto the image and colocalized with the particles. In support of the hypothesis, penetration of the tissue with NPs is greater in the alveolar regions than in the terminal bronchiolar regions. Clearly, though, the NPs are not uniformly distributed in alveoli but are more heavily localized in the acinar region near the TB.

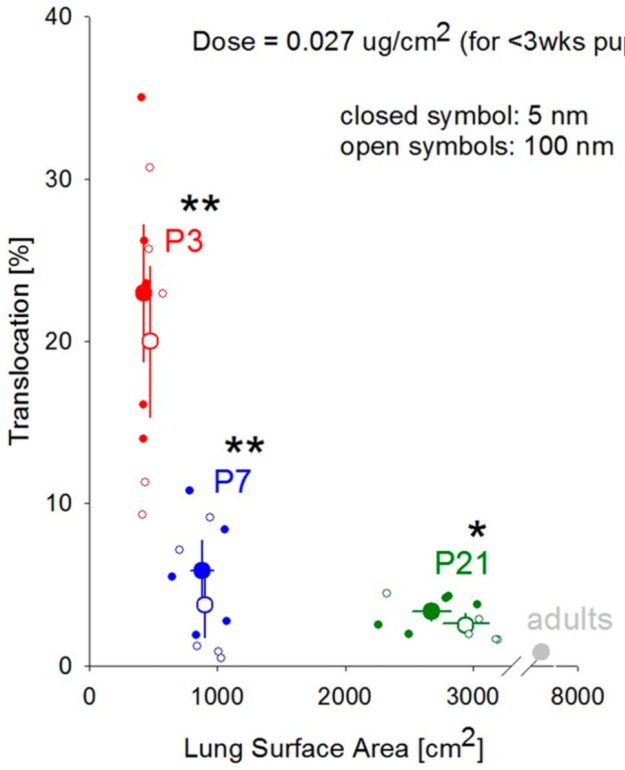

Figure 3.

Enhanced NP translocation from air to blood in the developing lungs. The amounts of gold in the lungs and in extrapulmonary tissues were measured by inductively coupled plasma mass spectrometry (ICP-MS), and from the ratio of these two values, the translocation efficiency was calculated and plotted against lung surface area. Red symbols are data from 3-day-old rats, blue symbols from 7-day-old rats, and green symbols from 21-day-old rats. The closed symbols represent treatment with 5 nm AuNPs; open symbols represent treatment with 100 nm AuNPs. At least five animals were studied for each age group and each treatment. Three adult animals (gray) were studied to document that the fraction of NPs translocating in adult animals is very small compared to that in neonates. We did not aim to repeat previous studies on NP translocation in adult animals,[8,12,13] which reported size dependency. The large symbols represent the average of each age group with translocation and lung surface area variation (standard deviation). Statistical significance was determined by ANOVA. Asterisk shows statistical significance compared to translocation in adult rats; double asterisks represent $P < 0.01$; a single asterisk represents $P < 0.05$. Pairwise comparisons were performed as needed by Tukey's test. Segmented regression[14,15] shows the lack of difference in the translocation between 5 nm *versus* 100 nm AuNPs in the developing lungs.

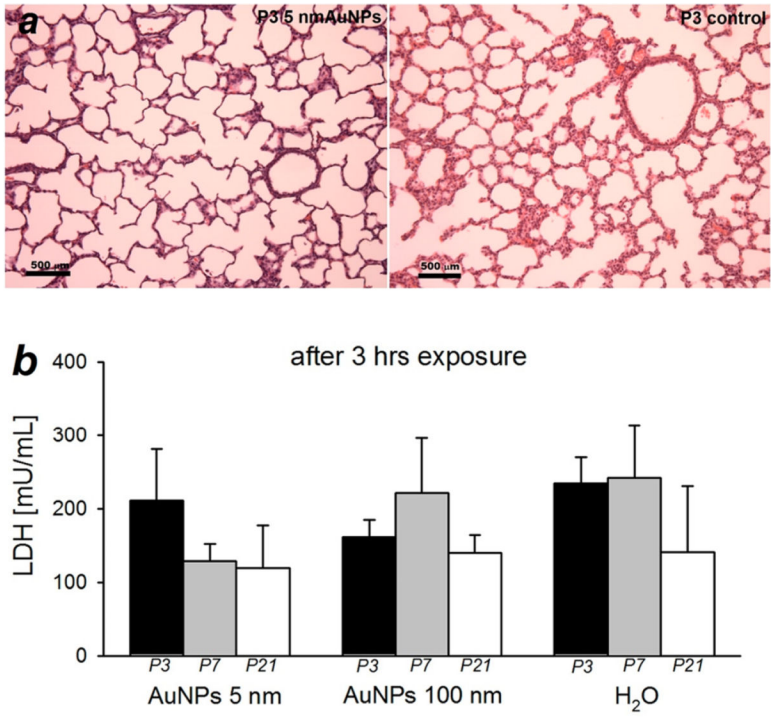

Figure 4.

NP exposure by instillation does not cause lung injuries. (a) Histopathology (HE staining) of the lung parenchyma of 5 nm NP-exposed (upper left) and unexposed (upper right) 3-day-old rats. (b) After 3 h of exposure to either 5 nm AuNPs, 100 nm AuNPs, or no NPs (control), 3-day-old, 7-day-old, and 21-day-old rats were sacrificed, and lactate dehydrogenase (LDH) was measured in lung lavage fluid as a readout of epithelial tissue damage. The bars show average (+) SD LDH activity, $n = 5$. No significant differences in LDH release are seen between the groups.

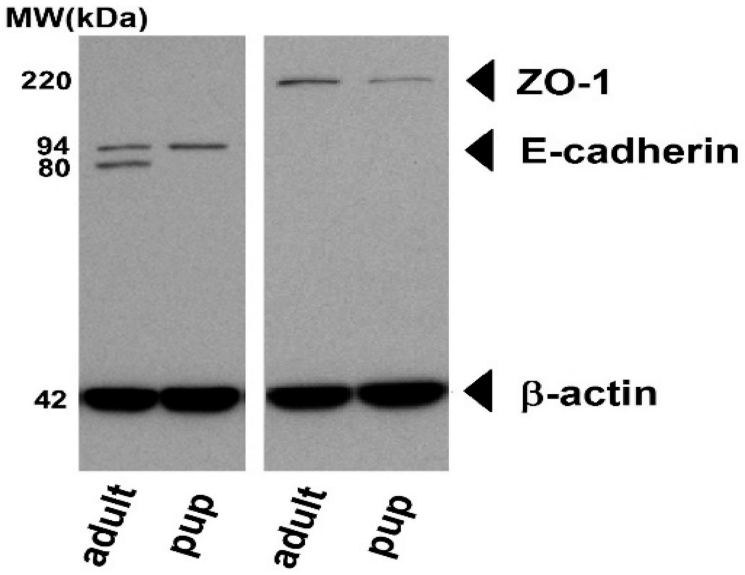

Figure 5.

Representative Western blot of excised lung tissue from adult rats and from 7-day-old rats. Left: E-cadherin-specific antibodies visualize the proE-cadherin precursor protein (94 kDa) and the functionally active mature E-cadherin polypeptide (80 kDa). Right: Expression of zonula occludens-1 (ZO-1) protein. The 43 kDa bands at the bottom show beta actin expression.